CTP#2722 April, 1998

Relativistic y-scaling and the Coulomb sum rule in nuclei

M. B. Barbaro[(a)], R. Cenni[(b)], A. De Pace[(a)], T. W. Donnelly[(c)] and A. Molinari[(a)]

(*a*) *Dipartimento di Fisica Teorica, Università di Torino and*
Istituto Nazionale di Fisica Nucleare, Sezione di Torino,
via P.Giuria, I-10125 Torino, Italy

(*b*) *Dipartimento di Fisica, Università di Genova and*
Istituto Nazionale di Fisica Nucleare, Sezione di Genova,
via Dodecaneso, I-16146 Genova, Italy

(*c*) *Center for Theoretical Physics, Laboratory for Nuclear Science and Department of Physics,*
Massachusetts Institute of Technology,
Cambridge, Massachusetts 02139

Abstract

In this paper dividing factors G_L and G_T are constructed for the longitudinal and transverse responses of the relativistic Fermi gas in such a way that the reduced responses so obtained scale. These factors parallel another dividing factor studied previously, H_L, that yields a (different) reduced response which fulfills the Coulomb sum rule. G_L, G_T and H_L are all found to be only very weakly model-dependent, thus providing essentially universal dividing factors. To explore the residual degree of dependence which remains, the scaling and sum rule properties of several specific models have been considered. It is seen that the relativistic Fermi gas (by construction) and also typical shell-model reduced responses successfully scale and satisfy the Coulomb sum rule, as do experimental results at medium to high momentum transfers. On the other hand, it is observed that the quantum hadrodynamic model does so only if interaction effects become weaker with increasing momentum transfer, as predicted in the most recent versions of that model.

I. INTRODUCTION: REDUCED RESPONSE FUNCTIONS

Motivated by our recent work [1,2] on the Coulomb sum rule (CSR), in this paper we return to the related problem of y-scaling. In Refs [1] we devised a factor H_L that, upon being divided into the longitudinal response function for quasielastic electron scattering, R_L, produced a so-called reduced response,

$$r_L \equiv R_L/H_L, \tag{1.1}$$

with convenient energy-weighted moments. Our approach started from the relativistic Fermi gas (RFG) model in which the moments are well understood. Specifically, the zeroth energy-weighted moment is the familiar CSR and becomes unity, that is, by construction is saturated exactly in the non-Pauli-blocked region where the momentum transfer $q > 2k_F$, with k_F the Fermi momentum. While the derivation of H_L provided in our previous studies was initially undertaken within the context of the RFG, we also showed that this dividing factor is only very weakly model-dependent, i.e., is essentially universal.

A first motivation in the present work is to re-cast the ideas involved in studying the behavior of the quasielastic response in the region where the energy transfer ω is lower than its value at the quasielastic peak, namely, in the so-called scaling region. Below we start by summarizing the basic ideas behind the concept of y-scaling [3,4] in which one attempts to find some function of q and ω, here denoted G, which, when divided into the inclusive electron scattering cross section, yields yet another reduced response with special properties. Namely, for an appropriately chosen scaling variable y (a well-defined function of q and ω; see below), this reduced response is a function only of q and y, denoted $F(q,y)$, and scales. The latter means that for sufficiently large momentum transfers the function becomes universal, namely a function only of the scaling variable y:

$$F(q,y) \stackrel{q\to\infty}{\longrightarrow} F(y) \equiv F(\infty,y). \tag{1.2}$$

The arguments for choosing the dividing function and scaling variable may be presented from various points of view, always with the goal of removing the single-nucleon content from the nuclear responses in as model-independent a manner as possible while still retaining essential relativistic effects whenever feasible. In Sec. IIA we review the usual approach [3] based on the Plane-Wave Impulse Approximation (PWIA). This yields the standard form of y and $F(q,y)$. Following this review, in Sec. IIB we re-cast our previous treatments of scaling [5] in terms of a related dimensionless variable ψ which arises naturally when studying the RFG model. In the present work we show how ψ is directly connected to a dimensionful variable $y_{\rm RFG}$, which for the RFG model is the analog of the usual y-variable. Thus, scaling behavior can be examined in terms of y, $y_{\rm RFG}$ or ψ. Each approach introduces specific functions by which the inclusive cross section or the individual longitudinal and transverse response functions, R_L and R_T, are to be divided to yield reduced responses F, F_L and F_T, respectively. In analogy with the previous treatment of the CSR, these dividing functions are denoted G, G_L and G_T, respectively; that is, for example

$$F_L \equiv R_L/G_L \tag{1.3}$$

$$F_T \equiv R_T/G_T. \tag{1.4}$$

In presenting results in Sec. III we show that, as was found to be the case for the dividing factor H_L, the dividing factors obtained in the scaling analysis are also only very weakly model-dependent. Indeed, in recent work medium- and high-energy data have been tested with both the usual y-scaling approach [3] and also the RFG-motivated approach [6] and seen to scale successfully (see also [7] for an analysis of all existing data). Additionally, it now appears that the experimental CSR is reasonably well saturated at high momentum transfers [8].

The second motivation for the present work is to put several models to the test, examining both their CSR behavior and their ability to scale. Clearly the RFG model has both properties, by construction. We also examine two other models of the quasielastic response (see Sec. IIC), the hybrid model (HM) introduced in Ref. [1] and the quantum hadrodynamic model (QHD) discussed in Refs. [9,10], to test how well they satisfy the CSR and are able to yield scaling behavior at high q. Each contains specific types of interaction effects that go beyond the strict RFG model and thus some violation of scaling and inability to yield a CSR of unity are to be expected. Our goal is to quantify the size of such effects and to explore whether or not the (successful) experimental behaviors can be used to constrain the models (see Sec. III).

Finally, in Sec. IV we return to summarize our findings from this study.

II. FORMALISM

A. The reduced response function F and scaling

We begin the discussion of the formalism with the most familiar chain of logic in which scaling is motivated within the context of the PWIA for $(e,e'N)$ reactions [3,4]. Since in this approach one uses the integrals over $(e,e'p)$ and $(e,e'n)$ cross sections to approximate the inclusive (e,e') cross section, one may begin by performing the average of the electron-nucleon cross section over the azimuthal angle of the ejected nucleon:

$$\bar{\sigma}_{eN}(q,\omega;p,\mathcal{E}) = \frac{1}{2\pi}\int d\phi_{\boldsymbol{N}}\sigma_{eN}(q,\omega;p,\mathcal{E};\phi_{\boldsymbol{N}}), \tag{2.1}$$

where $p=|\boldsymbol{p}|$ is the missing momentum and $\mathcal{E}$ the missing energy up to an offset of the (constant) separation energy $E_S = m_N + M^0_{A-1} - M^0_A$. Here m_N is the nucleon mass, M^0_A is the target mass and M^0_{A-1} is the mass of the daughter nucleon when in its ground state (see Ref. [1] for the notation adopted in this work). Traditionally one uses some off-shell prescription for the electron-nucleon cross section, e.g., the "cc" prescriptions of De Forest [11].

Next one defines the scaling variable. The exact kinematics (i.e., no PWIA modeling is involved — only the imposition of energy-momentum conservation on the $(e,e'N)$ process is required) permit one to say that the smallest value of the missing momentum attained in the so-called y-scaling region, the low-ω side of the quasielastic peak, occurs at $p_{min} \equiv -y$, where [3]

$$y = \frac{1}{2W^2}\left\{\left(M^0_A+\omega\right)\sqrt{W^2-\left(M^0_{A-1}+m_N\right)^2}\sqrt{W^2-\left(M^0_{A-1}-m_N\right)^2}\right.$$

$$- q\left[W^2 + \left(M^0_{A-1}\right)^2 - m_N^2\right]\Big\} \tag{2.2}$$

with

$$W = \sqrt{\left(M^0_A + \omega\right)^2 - q^2}. \tag{2.3}$$

The energy transfer is, of course, then given as a function of q and y. In particular, it must lie in the range [1] $\omega_t \leq \omega \leq q$, where

$$\omega_t = E_S + \sqrt{(M^0_{A-1} + m_N)^2 + q^2} - (M^0_{A-1} + m_N) \tag{2.4}$$

is the threshold energy. The scaling variable vanishes when

$$\omega = \omega_0 = E_S + \sqrt{m_N^2 + q^2} - m_N, \tag{2.5}$$

which is roughly the position of the quasielastic peak, and hence the scaling region is characterized by having y negative. It should be stressed that no approximation is involved in using (q, y) as the inclusive scattering variables rather than (q, ω), as they are related in a well-defined way through Eqs. (2.2,2.3). In discussions of quasielastic scattering the former usually proves to be more convenient, since the peak is found near $y = 0$, providing the best reference point for energy transfer at constant momentum transfer.

The next step usually involves making two approximations. In the first, one assumes that protons and neutrons are distributed the same way in the nucleus, presumably a reasonable approximation for the $N = Z$ nuclei considered in this work. Consequently one is assuming at this point that the spectral function of the nucleus does not carry any isospin index and that all such dependence can be incorporated in the overall eN cross section,

$$\tilde{\sigma}_{eN}(q, \omega; p, \mathcal{E}) \equiv \frac{E_N}{q}\left\{Z\bar{\sigma}_{ep}(q, \omega; p, \mathcal{E}) + N\bar{\sigma}_{en}(q, \omega; p, \mathcal{E})\right\}, \tag{2.6}$$

where the kinematic factor E_N/q with $E_N = ((\boldsymbol{q} + \boldsymbol{p})^2 + m_N^2)^{1/2}$ has been included, as in Ref. [3].

Following this one attempts to remove this effective eN cross section from under the integrals over missing energy and missing momentum involved in going from coincidence to inclusive scattering. The usual argument is to assume that the most important contributions to the nuclear spectral function arise for the lowest values of $(p, \mathcal{E})$ that can be reached for given values of q and y; in the scaling region these are $\mathcal{E} = 0$ and $p = -y$. Thus, in this approximation, the function one hopes will scale as a function of y when $q \to \infty$ is given by

$$F(q, y) \equiv \frac{d^2\sigma/d\Omega_e d\omega}{\tilde{\sigma}_{eN}(q, y; p = -y, \mathcal{E} = 0)}. \tag{2.7}$$

In the PWIA where the coincidence cross section factorizes into the electron-nucleon cross section and the nuclear spectral function $\tilde{S}$ this quantity becomes

$$F(q, y) = 2\pi \int_{-y}^{Y} p\, dp\, \tilde{n}(q, y; p), \tag{2.8}$$

where

$$\tilde{n}(q,y;p) = \int_0^{\mathcal{E}^-} d\mathcal{E}\,\tilde{S}(p,\mathcal{E}). \tag{2.9}$$

Here the conventional definition of the spectral function's normalization is taken to be

$$\int d\boldsymbol{p} \int_0^\infty d\mathcal{E}\,\tilde{S}(p,\mathcal{E}) = 1. \tag{2.10}$$

For the definition of the upper limits of integration in Eqs. (2.8) and (2.9) we refer the reader to Refs. [3] and [1]. Here we quote only the asymptotic results:

$$\lim_{q\to\infty} Y(q,\omega) = \infty \tag{2.11}$$

and

$$\lim_{q\to\infty} \mathcal{E}^-(q,y;p) = y + p - \left(\sqrt{M_{A-1}^{0^2} + p^2} - \sqrt{M_{A-1}^{0^2} + y^2}\right). \tag{2.12}$$

One sees that in the limit as $q \to \infty$ the result in Eq. (2.12) becomes independent of q and hence that the expression in Eq. (2.8) becomes a function only of y, namely, it scales.

B. The reduced responses F_L^{RFG} and r_L^{RFG}

Turning now to the RFG model, we have for its spectral function [1]

$$\tilde{S}^{\rm RFG}(p,\mathcal{E}) = \frac{3A}{8\pi k_F^3}\theta(k_F - p)\delta\left[\mathcal{E}(p) - \mathcal{E}^{\rm RFG}(p)\right], \tag{2.13}$$

where

$$\mathcal{E}^{\rm RFG}(p) = \left(\sqrt{k_F^2 + m_N^2} - \sqrt{p^2 + m_N^2}\right) \tag{2.14}$$

and where the usual convention is followed here of normalizing this spectral function to $Z = N = A/2$:

$$\int d\boldsymbol{p} \int_0^\infty d\mathcal{E}\,\tilde{S}^{\rm RFG}(p,\mathcal{E}) = A/2 \tag{2.15}$$

(note the different normalization from the one assumed above). For the physical responses discussed below, at the end of any calculation we, of course, take $A \to \infty$ in the strict RFG model. Defining the RFG scaling variable through the intercept of the support of the RFG spectral function given in Eq. (2.13) and the kinematical boundaries in the missing energy-missing momentum plane (see Ref. [1]) we obtain

$$y_{\rm RFG} = m_N\zeta = m_N\left(\lambda\sqrt{1 + \frac{1}{\tau}} - \kappa\right), \tag{2.16}$$

where, as in our past work, the dimensionless variables $\lambda = \omega/2m_N$, $\kappa = q/2m_N$ and $\tau = \kappa^2 - \lambda^2$ have been introduced. The RFG scaling variable in Eq. (2.16) vanishes for

$$\lambda = \lambda_0 = \frac{1}{2}\left[\sqrt{1+4\kappa^2} - 1\right] \ , \tag{2.17}$$

namely at $(\omega_0 - E_S)/2m_N$, the value previously obtained shifted by the separation energy (usually a small effect, and one that can be incorporated as in our past work [1]). The different choice of scaling variable made here is motivated through the observation that, as we have chosen to describe heavy nuclei rather than few-body systems, we expect the main strength in the nuclear spectral function to be found not at the lowest values of p and $\mathcal{E}$ that are accessible, as is indeed the case for few-body nuclei, but rather for values of $(p, \mathcal{E})$ determined (largely) by the dynamics of nucleons in other than the $1s$-shell.

Let us next close a logical loop and connect the RFG scaling variable defined above to the one originally proposed for the RFG [5] and referred to as ψ. The latter, in the non-Pauli-blocked region, has the following equivalent forms:

$$\begin{aligned}
\psi &= \frac{1}{\sqrt{\xi_F}}\left[2\theta(\lambda-\lambda_0)-1\right]\left\{\sqrt{(1+\lambda)^2 + \frac{1}{\tau}(\tau-\lambda)^2} - (1+\lambda)\right\}^{\frac{1}{2}} \\
&= \frac{1}{\sqrt{\xi_F}}\left[2\theta(\lambda-\lambda_0)-1\right]\left\{\kappa\sqrt{1+\frac{1}{\tau}} - (1+\lambda)\right\}^{\frac{1}{2}} \\
&= \frac{1}{\sqrt{\xi_F}}\frac{\lambda-\tau}{\sqrt{(1+\lambda)\tau + \kappa\sqrt{\tau(1+\tau)}}},
\end{aligned} \tag{2.18}$$

where $\xi_F = \epsilon_F - 1 = \sqrt{1+\eta_F^2} - 1$ and $\eta_F = k_F/m_N$ are the dimensionless Fermi kinetic energy and momentum, respectively. Both ψ and ζ vanish for $\lambda = \lambda_0$ and, by construction, for the RFG ψ is confined to lie in the range $-1 \leq \psi \leq 1$. It is straightforward to see that

$$\psi = \frac{\zeta}{\sqrt{\xi_F(1+\sqrt{1+\zeta^2})}} \tag{2.19}$$

which implies that

$$\xi_F\psi^2 = \sqrt{1+\zeta^2} - 1. \tag{2.20}$$

The physical significance of ψ is then immediately apparent: among the nucleons responding to an external probe one has the smallest kinetic energy and this is given by ψ^2 (in units of the dimensionless Fermi kinetic energy ξ_F).

We may now proceed as in the previous subsection and divide by a factor that is proportional to the sum of the ep and en cross sections, weighted by Z and N, respectively. From our previous work on the RFG model [5] we know that the azimuthal-angle-averaged eN cross section (compare Eq. (2.1)) is proportional to $v_L f_L + v_T f_T$, where v_L and v_T are the usual longitudinal and transverse Rosenbluth kinematical factors and, in terms of the electric $G_{Ep,n}$ and magnetic $G_{Mp,n}$ Sach's form factors, we have

$$f_L(\kappa,\lambda;\chi) = \frac{\kappa^2}{\tau}\left[Z(G_{Ep}^2 + W_{2p}\chi^2) + N(G_{En}^2 + W_{2n}\chi^2)\right] \tag{2.21}$$

$$f_T(\kappa,\lambda;\chi) = Z(2\tau G_{Mp}^2 + W_{2p}\chi^2) + N(2\tau G_{Mn}^2 + W_{2n}\chi^2) \tag{2.22}$$

with

$$W_{2p,n}(\tau) = \frac{1}{1+\tau}\left[G_{Ep,n}^2(\tau) + \tau G_{Mp,n}^2(\tau)\right]. \tag{2.23}$$

Here $\chi \equiv \eta\sin\theta$, where $\eta \equiv p/m_N$ and θ is the angle between $\mathbf{p}$ and $\mathbf{q}$. Note that the δ-function in Eq. (2.13) requires that $\mathcal{E} = \mathcal{E}^{\rm RFG}$ as defined in Eq. (2.14).

We could proceed to follow exactly the procedures outlined in the previous subsection, working from the unseparated inclusive cross section towards a reduced response which, if successful, would scale as $q \to \infty$. Instead, in this work for the most part we work directly with the separated longitudinal and transverse responses, R_L and R_T, respectively, since (1) we are most interested in model-to-model comparisons and the same procedures may be followed in each case (i.e., focusing on L or T responses directly), (2) a few cases exist where L/T separations have been performed experimentally, and (3) we wish to draw comparisons with studies of the Coulomb sum rule where only the L response is relevant. In fact, in most of the discussions to follow we shall limit our attention to the longitudinal channel and only give a few results for the transverse case.

We now seek reduced responses denoted $F_{L,T}(\kappa,\psi)$ that scale. These are to be obtained from the inclusive response functions $R_{L,T}(\kappa,\lambda)$ by dividing through by specific functions denoted $G_{L,T}(\kappa,\lambda)$ (discussed below):

$$F_{L,T}(\kappa,\psi) \equiv R_{L,T}(\kappa,\lambda)/G_{L,T}(\kappa,\lambda). \tag{2.24}$$

If the dividing functions are chosen appropriately, then as above the reduced responses defined in Eq. (2.24) will scale, namely, become functions only of a single scaling variable such as ψ defined above when $\kappa \to \infty$,

$$F_{L,T}(\kappa,\psi) \stackrel{\kappa\to\infty}{\longrightarrow} F_{L,T}(\psi) \equiv F_{L,T}(\infty,\psi). \tag{2.25}$$

To obtain the dividing functions we proceed from the spectral function for the RFG, using the general PWIA expressions given above. Let us first focus on the longitudinal response. With Eq. (2.13) we have

$$\tilde{n}^{\rm RFG}(q,y_{\rm RFG},p) = \int_0^{\mathcal{E}^-} d\mathcal{E}\,\tilde{S}^{\rm RFG}(p,\mathcal{E}) = \frac{3A}{8\pi k_F^3}\theta(k_F-p)\theta(p+y_{\rm RFG}) \tag{2.26}$$

and therefore, from Eq. (2.8), together with a factor $Z = N = A/2$ to account for the different normalizations of $\tilde{S}$ and $\tilde{S}^{\rm RFG}$, we have

$$F_L^{\rm RFG}(q,y_{\rm RFG}) \equiv F_L^{\rm RFG}(y_{\rm RFG}) = \frac{3}{2k_F^3}\int_{-y_{\rm RFG}}^{k_F} p\,dp = \frac{3}{4k_F^3}(k_F^2 - y_{\rm RFG}^2). \tag{2.27}$$

By exploiting Eq. (2.20) it is then an easy matter to obtain

$$k_F^2 - y_{\rm RFG}^2 = m_N^2 \xi_F (1-\psi^2)[2 + \xi_F(1+\psi^2)] \tag{2.28}$$

and hence the scaling function of the RFG will read

$$F_L^{\rm RFG}(\psi) = \frac{3\xi_F}{2m_N\eta_F^3}(1-\psi^2)\theta(1-\psi^2)\left[1 + \frac{1}{2}\xi_F(1+\psi^2)\right]. \tag{2.29}$$

We now recall from previous work [5] that the RFG longitudinal response function is given by (see Fig. 1)

$$R_L^{\rm RFG}(\kappa,\lambda) = \frac{3\xi_F}{4m_N\kappa\eta_F^3}[ZU_{Lp} + NU_{Ln}](1-\psi^2)\theta(1-\psi^2), \tag{2.30}$$

where the nucleonic terms $U_{Lp,n}$ are the following:

$$U_{Lp,n} = \frac{\kappa^2}{\tau}\left[G_{Ep,n}^2(\tau) + W_{2p,n}(\tau)\Delta\right]. \tag{2.31}$$

Furthermore Δ, which, in the non-Pauli-blocked domain, reads

$$\Delta = \frac{\tau}{\kappa^2}\left[\frac{1}{3}\left(\epsilon_F^2 + \epsilon_F\sqrt{1+\zeta^2} + 1 + \zeta^2\right) + \lambda\left(\epsilon_F + \sqrt{1+\zeta^2}\right) + \lambda^2\right] - (1+\tau), \tag{2.32}$$

represents the transverse component (with respect to $\boldsymbol{q}$) of the momentum of the struck nucleon [2]. It follows that the required RFG dividing function is given by

$$G_L(\kappa,\lambda) = \frac{ZU_{Lp} + NU_{Ln}}{2\kappa[1 + \xi_F(1+\psi^2)/2]} \tag{2.33}$$

$$= \frac{1}{2\kappa}(ZU_{Lp} + NU_{Ln}) + \mathcal{O}(\xi_F), \tag{2.34}$$

telling us that the scaling function of the RFG arises from R_L not only by pulling out the non-scaling single-nucleon factor involving U_{Lp}/κ and U_{Ln}/κ, but also contains a small correction for the medium dependence in the problem (the factor in the denominator involving ψ). Typically ξ_F is very small, attaining values as large as 0.04 only in the heaviest of nuclei, and thus both the correction in the denominator containing ξ_F and the medium-dependent effects in the numerator embodied in Δ provide only few percent corrections at high momentum transfers, as long as ψ is not permitted to become large. Indeed, in the RFG its magnitude is bounded by unity and so this always obtains at high q; if the ideas here are carried over to other models where large excursions away from the quasielastic peak are permitted, then one should check the actual size of these medium-dependent corrections.

Dividing the longitudinal response function by G_L then yields the reduced response F_L which, at least for the RFG, scales with ψ, ζ or $y_{\rm RFG}$. Note that we can use Eq. (2.20) to write

$$1 + \frac{1}{2}\xi_F(1+\psi^2) = \frac{1}{2}\left(\epsilon_F + \sqrt{1+\zeta^2}\right), \tag{2.35}$$

giving us some insight into the physical significance of the denominator in Eq. (2.34): namely, it represents an average energy of the nucleons responding to the external probe.

Proceeding in exactly the same way for the transverse channel it is straightforward to see that the dividing factor required in discussions of scaling in that case is

$$G_T(\kappa,\lambda) = \frac{ZU_{Tp}+NU_{Tn}}{2\kappa[1+\xi_F(1+\psi^2)/2]} \tag{2.36}$$

$$= \frac{1}{2\kappa}(ZU_{Tp}+NU_{Tn}) + \mathcal{O}(\xi_F), \tag{2.37}$$

where (compare Eq. (2.22))

$$U_{Tp,n} = 2\tau G^2_{Mp,n}(\tau) + W_{2p,n}(\tau)\Delta. \tag{2.38}$$

The unseparated responses may then be analyzed using

$$F(\kappa,\psi) \equiv \frac{d^2\sigma/d\Omega_e d\omega}{\sigma_M[v_L G_L(\kappa,\lambda)+v_T G_T(\kappa,\lambda)]}, \tag{2.39}$$

where as usual one would have for the cross section

$$d^2\sigma/d\Omega_e d\omega = \sigma_M[v_L R_L(\kappa,\lambda)+v_T R_T(\kappa,\lambda)] \tag{2.40}$$

with σ_M the Mott cross section and $v_{L,T}$ the usual Rosenbluth kinematical factors. Naturally, in the RFG model we have $F^{\rm RFG} = F^{\rm RFG}_T = F^{\rm RFG}_L$, the result being given in Eq. (2.29).

The developments presented here for scaling have been motivated by our previous discussions of the Coulomb sum rule and various energy-weighted moments of another reduced response denoted $r_L(\kappa,\lambda)$ [1,5]. In those studies the longitudinal response $R_L(\kappa,\lambda)$ was divided by a function $H_L(\kappa,\lambda)$ to yield

$$r_L(\kappa,\psi) \equiv R_L(\kappa,\lambda)/H_L(\kappa,\lambda), \tag{2.41}$$

where the nth moment of the longitudinal response of the nucleus is given by

$$\Xi^{(n)} = \int_0^\kappa d\lambda\, \lambda^n\, r_L(\kappa,\lambda). \tag{2.42}$$

In particular, the $n=0$ moment, $\Xi^{(0)}$, is the Coulomb sum rule. In the case of the RFG our previous work showed that

$$H_L(\kappa,\lambda) = \frac{ZU_{Lp}+NU_{Ln}}{J_L}, \tag{2.43}$$

where $U_{Lp,n}$ are given above and where

$$J_L = \frac{\kappa\eta_F^3}{2\xi_F}\frac{\partial\psi}{\partial\lambda} \tag{2.44}$$

$$= \left(\frac{\kappa^2}{\tau}\right)\left(\frac{1+2\lambda}{1+\lambda}\right) + \mathcal{O}(\xi_F). \tag{2.45}$$

Thus, by dividing the charge response of the RFG by Eq. (2.43) (see Eq. (2.30)) one obtains the following reduced longitudinal response

$$r_L^{\rm RFG}(\kappa,\lambda) = \frac{3}{8m_N}(1-\psi^2)\theta(1-\psi^2)\frac{\partial\psi}{\partial\lambda}, \tag{2.46}$$

which, by construction, fulfills the CSR in the non-Pauli-blocked domain, as can easily be verified. Observe also that while $F_L^{\rm RFG}$ attains its maximum for $\psi = 0$, i. e. for $\lambda = \lambda_0$, this is nearly, but not exactly, true for $r_L^{\rm RFG}$ only for small values of η_F. Indeed using the simple expression

$$\psi \cong \frac{1}{\eta_F}\left[\frac{\lambda(\lambda+1)}{\kappa} - \kappa\right], \tag{2.47}$$

which approximates Eq. (2.18) quite faithfully for very large values of κ except on the borders of the response region, it turns out that the maximum of $r_L^{\rm RFG}$ occurs at

$$\lambda = \frac{1}{2}\left[\sqrt{1+4\kappa^2\left(1+\frac{1}{\sqrt{5}}\frac{\eta_F}{\kappa}\right)} - 1\right] = \lambda_0 + \mathcal{O}(\eta_F^2). \tag{2.48}$$

Before leaving this discussion of the RFG model reduced responses, for completeness let us mention another version of the reduced longitudinal response that can be obtained in terms of the variable ζ rather than ψ as in (2.41). For this purpose one has to divide Eq. (2.30) by Eq. (2.43) with J_L replaced by

$$J_L' = \frac{2\kappa\eta_F^2}{3}\frac{\partial\zeta}{\partial\lambda}\frac{1}{\epsilon_F - \dfrac{\sinh^{-1}\eta_F}{\eta_F}}. \tag{2.49}$$

The result is

$$r_L^{\rm RFG'}(\kappa,\lambda) = \frac{1}{2m_N\eta_F}\frac{\epsilon_F - \sqrt{1+\zeta^2}}{\epsilon_F - \dfrac{\sinh^{-1}\eta_F}{\eta_F}}\theta(\eta_F - |\zeta|)\frac{\partial\zeta}{\partial\lambda}, \tag{2.50}$$

which again fulfills the CSR. Indeed

$$\Xi^{(0),{\rm RFG}} = \int_0^\kappa d\lambda\, r_L^{\rm RFG'}(\kappa,\lambda) = \frac{1}{\eta_F}\frac{1}{\left(\epsilon_F - \dfrac{\sinh^{-1}\eta_F}{\eta_F}\right)}\int_{-\eta_F}^{\eta_F} d\zeta\left(\epsilon_F - \sqrt{1+\zeta^2}\right) = 1. \tag{2.51}$$

C. Scaling and sum rules in the HM and QHD models

An extension of the RFG to account for the binding of the nucleons inside the nucleus, thus curing a flaw of the RFG related to its negative separation energy, is represented by the hybrid model studied previously in Ref. [1]. The HM has continuum states which are simply

plane waves, as in the RFG model, but has bound states described by shell-model wave functions obtained by solving the Schrödinger equation with some choice of potential well. For simplicity in studying the $A \to \infty$ limit, in [1] we chose to consider harmonic oscillator bound-state wave functions. The longitudinal response $R_L^{\rm HM}$ is also shown in Fig. 1.

In the HM scaling variables which incorporate the shift result from using Eq. (2.16) for ζ' (and a corresponding dimensionful variable y') or Eq. (2.18) for ψ' by making the replacements $\lambda \to \lambda'$ and $\tau \to \tau' = \kappa^2 - \lambda'^2$, where

$$\lambda' = \lambda - \lambda_{\rm shift}, \tag{2.52}$$

being

$$\lambda_{\rm shift} = \frac{1}{2m_N}(T_F + E_S) \tag{2.53}$$

and $T_F = \sqrt{k_F^2 + m_N^2} - m_N = m_N \xi_F$ the Fermi kinetic energy. The HM turns out to have the width of its reduced response (its variance, see Ref. [1]) identical to a RFG computed with a Fermi momentum somewhat larger than the usual one (237 MeV/c for the HM, versus the 230 MeV/c value for k_F used here for the RFG to correspond to nuclei near ^{40}Ca or ^{56}Fe). In conformity, ψ' should be computed with k_F=237 MeV/c as well. As seen in Fig. 1, the shift arising from replacing λ with $\lambda_{\rm shift}$ according to Eq. (2.53) is apparent.

Scaling may then be examined for the HM by computing

$$F_L^{\rm HM}(\kappa, \psi) \equiv R_L^{\rm HM}(\kappa, \lambda)/G_L(\kappa, \lambda) \tag{2.54}$$

and the various energy-weighted moments of the longitudinal response, including the zeroth moment or CSR, may be computed using

$$r_L^{\rm HM}(\kappa, \psi) \equiv R_L^{\rm HM}(\kappa, \lambda)/H_L(\kappa, \lambda). \tag{2.55}$$

Note that we have used the *same* dividing factors G_L and H_L that were developed from our discussions of the RFG in the previous subsection. In [1] we showed that H_L is universal in that the form found for the HM essentially coincides with the one obtained above. In the next section we present results where the corresponding universality of G_L is tested numerically. Naturally these explorations also involve displaying the reduced responses given in Eqs. (2.54) and (2.55) as functions of ψ' as well as ψ.

Finally we turn to an examination of the QHD model [9]. In this model protons and neutrons in the nucleus are described by Dirac spinors and move in strong Lorentz scalar and vector mean fields. These in turn arise self-consistently from the exchange of σ and ω mesons between the same nucleons on which they act. The scalar field dresses the bare mass of the nucleon, considerably lowering its value; the vector field uniformly shifts the fermion spectrum. As a consequence the QHD charge response of nuclear matter in Hartree approximation is unaffected by the vector field, while it turns out to be quite sensitive to the effective mass m_N^* induced by the scalar field, as shown in Ref. [10]. This is, of course, true in the simple approximation of constant relativistic mean fields. An improved description allows for an energy dependence of the latter which helps to account for the

data of proton-nucleus elastic scattering. We shall however ignore these refinements in the present analysis.

In Fig. 1, in order to directly compare with the results of Ref. [10], we display the longitudinal response of nuclear matter, again using $k_F = 230$ MeV/c, in the Hartree version of QHD for $q = 0.55$ and 1.14 GeV/c, respectively. In addition to the RFG and HM results discussed above, here we also show curves corresponding to $m_N^* = 0.8\, m_N$ and $m_N^* = 0.68\, m_N$, namely, those displayed in Ref. [10] for the case of constant relativistic mean fields. From the figure the sensitivity of the charge response to m_N^* is fully apparent. Clearly the more m_N^* deviates from m_N the more the longitudinal QHD response is hardened (shifted to higher values of ω). The most recent version of QHD suggests that as q increases the effective value of m_N^* should tend towards m_N and thus that, for intermediate-energy studies ($q \sim 500$ MeV/c), m_N^*/m_N may be somewhere between 0.68 and 0.8, while for high q, a value between 0.8 and 1.0 is likely to be preferred.

As above for the HM model, scaling will be examined in the QHD model by computing

$$F_L^{\rm QHD}(\kappa, \psi) \equiv R_L^{\rm QHD}(\kappa, \lambda)/G_L(\kappa, \lambda) \tag{2.56}$$

and likewise the various energy-weighted moments of the longitudinal response will be computed using

$$r_L^{\rm QHD}(\kappa, \psi) \equiv R_L^{\rm QHD}(\kappa, \lambda)/H_L(\kappa, \lambda), \tag{2.57}$$

where $R_L^{\rm QHD}(\kappa, \psi)$ is given below in Eq. (2.63). Our contention is that the dividing factors are (at least to a very good level of approximation; see Sec. III) universal and accordingly here we have continued to use the *same* dividing factors G_L and H_L that were developed from our discussions of the RFG in the previous subsection. In discussing the QHD results in the next section we shall display the reduced responses in Eqs. (2.56) and (2.57) as functions both of ψ and also ψ^*, namely, the RFG scaling variable given in Eq. (2.18) with m_N replaced by m_N^*. We shall also briefly explore what happens when the $m_N \to m_N^*$ replacement is made in a particular way to obtain modified dividing factors, G_L^* and H_L^*, defined below.

Before proceeding to reduce the QHD response a delicate point arises in connection with the question: does the concept of effective mass also apply to the single-nucleon content of the longitudinal response? The answer is yes and no. In fact the approach of Ref. [10] requires the Dirac F_1 and Pauli F_2/m_N form factors in the medium to be *identical* to those in free space (or, in other words, the nucleon current to be unaltered). Thus they are expressed in terms of the Sach's electric and magnetic form factors through the standard relations

$$F_{1p,n}(\tau) = \frac{1}{1+\tau}\left[G_{Ep,n}(\tau) + \tau G_{Mp,n}(\tau)\right] \tag{2.58a}$$

and

$$F_{2p,n}(\tau) = \frac{1}{1+\tau}\left[G_{Mp,n}(\tau) - G_{Ep,n}(\tau)\right], \tag{2.58b}$$

with $G_{Ep,n}$ and $G_{Mp,n}$ fitting the results of electron-nucleon elastic scattering in *free* space. Then, to keep $F_{1p,n}$ and $F_{2p,n}/m_N$ unaltered, the Sach's form factors in the medium should be given by

$$G^*_{Ep,n}(q,\omega) = F_{1p,n}(\tau) - \tau^* \frac{m^*_N}{m_N} F_{2p,n}(\tau), \tag{2.59a}$$

$$G^*_{Mp,n}(q,\omega) = F_{1p,n}(\tau) + \frac{m^*_N}{m_N} F_{2p,n}(\tau), \tag{2.59b}$$

where $\tau^* = (m_N/m^*_N)^2\tau$. Hence they will differ from the corresponding quantities in free space. Indeed it is the m^*_N appearing in Eq. (2.59b) that causes a strong reduction of the proton's convection current and, as a consequence, leads a considerable quenching of the magnetic moment of odd-proton-nuclei. To restore the agreement between the theoretical predictions of QHD and experiment a substantial back-flow current contribution has then to be invoked [12].

For the quasielastic charge response we face a similar situation. In fact, as discussed above, we reduce the QHD longitudinal response by using as dividing factors G_L and H_L defined in Eqs. (2.34) and (2.43), respectively, with the *bare* nucleon mass and, hence, with the *free* $G_{Ep,n}$ and $G_{Mp,n}$. An alternative might be to use $G^*_{Ep,n}$ and $G^*_{Mp,n}$ given above, together with

$$W^*_{2p,n}(q,\omega) = \frac{1}{1+\tau^*}\left(G^{*^2}_{Ep,n} + \tau^* G^{*^2}_{Mp,n}\right), \tag{2.60}$$

to define U^*_L using an expression that is analogous to Eq. (2.23). This would lead to dividing factors we denote G^*_L and H^*_L, and, by making the replacement $m_N \to m^*_N$ in Eq. (2.18), to a corresponding scaling variable ψ^*. Accordingly we would have different reduced responses (again labeled with an asterisk):

$$F^{\rm QHD*}_L(\kappa,\psi) \equiv R^{\rm QHD}_L(\kappa,\lambda)/G^*_L(\kappa,\lambda) \tag{2.61}$$

and

$$r^{\rm QHD*}_L(\kappa,\psi) \equiv R^{\rm QHD}_L(\kappa,\lambda)/H^*_L(\kappa,\lambda). \tag{2.62}$$

Clearly, since the QHD longitudinal response function is given by (compare with Eq. (2.30))

$$R^{\rm QHD}_L(\kappa,\lambda) = \frac{3\xi^*_F}{4m_N\kappa\eta^{*\,3}_F}[ZU^*_{Lp} + NU^*_{Ln}](1-\psi^{*2})\theta(1-\psi^{*2}) \ , \tag{2.63}$$

the reduced responses $F^{\rm QHD*}_L$ and $r^{\rm QHD*}_L$ will behave as functions of ψ^* exactly as $F^{\rm RFG}_L$ and $r^{\rm RFG}_L$ behave as functions of ψ. In the following section we return briefly to examine the consequences of these alternative definitions of the dividing factors.

III. RESULTS

We have thus reached the point at which the longitudinal reduced response functions F_L (for scaling discussions) and r_L (for sum-rule discussions) are to be obtained by dividing R_L by two different factors, G_L and H_L, respectively. The first is given by Eq. (2.34), while the second is given in Eq. (2.43) and they are related according to

$$G_L(\kappa,\lambda) = \left(\frac{\eta_F^3}{4\xi_F}\right)\frac{\partial\psi}{\partial\lambda}\frac{1}{1+\xi_F(1+\psi^2)/2}H_L(\kappa,\lambda) \tag{3.1}$$

$$= \frac{1}{2}\left(\frac{\kappa}{\tau}\right)\left(\frac{1+2\lambda}{1+\lambda}\right)H_L(\kappa,\lambda) + \mathcal{O}(\xi_F). \tag{3.2}$$

Naturally, the analogous dividing function G_T in Eq. (2.37) should be used when treating the separated transverse response or the combination $\sigma_M[v_L G_L(\kappa,\lambda) + v_T G_T(\kappa,\lambda)]$ in Eq. (2.39) may be used when dealing with an unseparated cross section. To assess the universality of using the various approaches discussed in the preceeding section, we show in Figs. 2 and 3 two mixed representations of the usual y-scaling results and the RFG-motivated results. In Fig. 2 the total RFG cross section is displayed divided by the De Forest cc1 off-shell result [11] — this is what is usually set as the dividing factor in presenting unseparated data in the form $F(q,y)$ versus y, as in Ref. [3]. Here we have taken $E_S = 8$ MeV as being typical of nuclei across the periodic table. Clearly once the momentum transfer is large enough (say above about 1 GeV/c) it is irrelevant whether the cc1 form is used or the RFG form is employed: the dividing factor is effectively universal. In Fig. 3 the usual reduced response for the RFG (i.e., with the dividing factor given in Eq. (2.39)) is displayed, however as a function of y rather than ψ, in which it of course scales perfectly. Again, at all but the lowest momentum transfer the scaling is excellent in y as well as ψ. These and other more extensive studies show that at high momentum transfers the choice of scaling variable is largely irrelevant, as long as one of the relativistic forms discussed in this work is employed, and that the on- and off-shell prescriptions for the dividing factors yield essentially model-independent results for scaling (as they did for the CSR).

By exploiting the essentially universal dividing factors H_L and G_L, we are thus in a position to test whether or not a given model fulfills the CSR and scales. Here we examine the longitudinal response functions of the HM [1] and QHD [9,10] models in concert with the RFG results obtained previously.

The response function $R_L^{\rm HM}$ of the hybrid model has been computed in Ref. [1] and, when divided by H_L, shown to satisfy the CSR. There, as already mentioned, it was seen that in setting up ψ' the effective Fermi momentum 237 MeV/c should be taken: the associated shift in λ (see Eq. (2.53)) turns out then to be $\lambda_{\rm shift} = 0.02$. Fixing G_L similarly, in Fig. 4 we display $F_L^{\rm HM}$ for ^{40}Ca versus ψ and ψ' for four different values of q (the RFG result is also shown for reference) and then display it in Fig. 5 versus q for $\psi = -0.1$ and -0.5, as well as for $\psi' = -0.1$ and -0.5. As seen in Fig. 4, the HM scales either with ψ or with ψ' as q becomes large; indeed, only the $q = 500$ MeV/c plot versus ψ shows any appreciable violation of scaling. Clearly (by construction) the scaling versus ψ' is excellent. It should also be noted that the final scaling result in the upper panel in Fig. 4 lies a little to the right of $\psi = 0$, while that in the lower panel lies a little to the left of $\psi' = 0$, suggesting that the value for $\lambda_{\rm shift}$ in Eq. (2.53) used here is somewhat too large and has led to an "overshooting" of the shift. Figure 5 shows the evolution of scaling with q and confirms that the asymptotic behavior has essentially been reached by about 1 GeV/c. We also see that the scaling sets in sooner when $|\psi'|$ is smaller, i.e., when one is closer to the quasielastic peak position.

In Figs. 6 and 7 we display $F_L^{\rm QHD}$ for ^{40}Ca versus ψ and ψ^* for four different values of q (the RFG result is also shown for reference) and then display it in Fig. 8 versus q for

$\psi = -0.1$ and -0.5, as well as for $\psi^* = -0.1$ and -0.5. Here results are shown both for $m_N^* = 0.68\, m_N$ and $0.8\ m_N$. The results in Figs. 6 and 7 show that $F_L^{\rm QHD}$ does not scale versus ψ when the effective mass is constant and differs from m_N. As q continues to grow beyond the range of values shown in the figures, the results continue to shift to higher ω and never coalesce into a universal curve (see also Fig. 8). When plotted versus ψ^* the behavior, while better, still does not scale. This is contrast with the RFG and HM results displayed above and, importantly, is not what is seen experimentally where the world data do appear to scale in ψ [7] (see also [6]). Comparing Figs. 6 and 7, it is clear that scaling is better when m_N^* is closer to m_N, indeed becoming perfect when $m_N^* \to m_N$, as expected, since then $F_L^{\rm QHD} \to F_L^{\rm RFG}$. The fact that experimentally the scaling is observed to occur successfully for q greater than about 1 GeV/c suggests that m_N^*/m_N should not deviate appreciably from unity for such kinematics.

In Fig. 9 the CSR associated with the QHD model is displayed for ^{40}Ca ($k_F = 230$ MeV/c) and for a set of values of m_N^* ranging from $0.5 m_N$ to the bare nucleon mass. Here we observe an effective mass dependence mostly due to the factor m_N^* in front of the CSR integral

$$\begin{aligned}
\Xi^{(0),{\rm QHD}} &= \int_0^q d\omega r_L^{\rm QHD}(q,\omega) \\
&= \frac{3}{4}\left(\frac{m_N^*}{m_N}\right)^3 \frac{\xi_F^*}{\xi_F} \int_{-1}^{1} d\psi^* \frac{U_L^*}{U_L}(1-\psi^{*^2})\frac{\partial\psi}{\partial\psi^*} \\
&\cong \frac{3}{4}\frac{m_N^*}{m_N} \int_{-1}^{1} d\psi^* \frac{U_L^*}{U_L}(1-\psi^{*^2})\frac{\partial\psi}{\partial\psi^*},
\end{aligned} \tag{3.3}$$

but also, to a less extent, to the Jacobian $\partial\psi/\partial\psi^*$. In fact, using Eq. (2.47), the latter can be cast in the form

$$\frac{\partial\psi}{\partial\psi^*} \cong 1 - \frac{1 - m_N^*/m_N}{\sqrt{1 + 4\kappa(\kappa + \eta_F\psi)}}, \tag{3.4}$$

which is less than unity for finite κ. These two factors, which are both clearly related to many-body aspects of the nuclear response, are however partially counteracted by the "single-nucleon term" U_L^*/U_L which is also m_N^* dependent and greater than unity. For large values of κ, Eq. (3.4) goes to one, whereas U_L^*/U_L continues to grow rapidly, increasingly so for smaller values of m_N^*. This then becomes the dominant factor in explaining the behavior of the curves in Fig. 9 for q, say, larger than 1 GeV/c.

As discussed above, the expectation is that m_N^* must evolve with q towards m_N. Thus, while at $q = 500$ MeV/c a value of $m_N^*/m_N \cong 0.7$ may be acceptable (implying that the resulting CSR will be about 5–10% below unity), as q reaches the higher values between 1 and 2 GeV/c, values of m_N^*/m_N nearer unity will be preferable from the point of view of scaling (and also suggested by the full version of QHD, see Ref. [10]) and will therefore yield a CSR that still remains close to unity.

For completeness, using the nomenclature introduced in Ref. [1], we display in Fig. 10 the CSR ($\Xi^{(0)}$), the energy-weighted sum rule ($\Xi^{(1)}/\Xi^{(0)}$) and the variance $\sigma = \sqrt{\Xi^{(2)} - (\Xi^{(1)})^2}$

of ^{40}Ca according to the HM, QHD (with $m_N^* = 0.68\ m_N$ and $0.8\ m_N$) and RFG models. As expected the responses of the HM and QHD models are considerably hardened with respect to that of the RFG; in addition the width of the QHD response is substantially wider than for the other two models.

In concluding this section we shortly discuss the scaling variables. In this paper four scaling variables have been introduced: the canonical y, the ψ of the RFG (together with its related variations, ζ and $y_{\rm RFG}$), the ψ' of the HM and the ψ^* of the QHD. How are they interrelated? To answer this question in Fig. 11 we display their behavior as functions of ω for $q = 1$ GeV/c. The following features emerge from the figure:

a) The behavior of the canonical y variable versus the mass number A is very rapid at small A and appears by $A = 20$ to have almost reached its asymptotic $A = \infty$ value.

b) In accord with the findings of [1], for large A, y is roughly given by Eq. (2.47) with λ shifted downward by an amount *grosso modo* corresponding to E_S. Hence in the $A = \infty$ limit one does not recover the RFG y-variable from y, but a slightly shifted result.

c) The variable ψ' is also shifted downward with respect to ψ, by an amount set by $\lambda_{\rm shift}$ in Eq. (2.53), although we conjecture (see above) that this shift is somewhat too large.

d) Finally, note the behavior of ψ^* with ω: it turns out to be shifted towards higher energies with respect to the other scaling variables. This goes in parallel with the energy-weighted sum rule of the QHD model whose reduced response is substantially hardened in comparison with other models here considered for $q \geq$500 MeV/c.

IV. FINAL COMMENTS

Our motivations in this work have been to study the Coulomb sum rule and scaling in a unified way, and to explore various models for the inclusive electromagnetic response of nuclei in the quasielastic region to see whether or not they simultaneously satisfy the CSR and scale. We have demonstrated how our previous work on the CSR may be generalized to include treatments of scaling: in both cases the response functions or the cross section are divided by specific functions, H_L for the CSR and G_L, G_T or $\sigma_M(v_L G_L + v_T G_T)$, as is appropriate, for scaling, to yield reduced responses with the desired properties, namely, a CSR or scaling behavior. We have studied the model-dependence of these dividing functions within the context of two specific models for the single-nucleon content in the problem and found it to be small, as long as we restrict our attention to high momentum transfers and to the vicinity of the quasielastic peak. Essentially, for such conditions, we have obtained nearly universal dividing functions with which any model can be tested and with which experimental data can be reduced. Typically we find corrections at high q which are characterized by $\eta_F^2 = (k_F/m_N)^2$, namely, reaching only $\sim$8% for the heaviest nuclei.

In the course of this study we have introduced and inter-related several types of scaling variables (y, ψ, ζ, $y_{\rm RFG}$, ψ'). These variables are all closely related: they differ at most by small shifts introduced by the various models to account (at some level) for interaction effects. On the one hand, when experimental data are reduced using our dividing functions, they are seen to yield a CSR at high-q and to scale when plotted versus any of the scaling variables listed above. On the other hand, the models considered in this work yield various results. The relativistic Fermi gas (RFG) model and the hybrid model (HM) both saturate

the CSR at high-q. In contrast, the quantum hadrodynamical (QHD) model does so only if the effective value of m_N^*/m_N evolves with increasing q towards unity, as suggested by the latest version of the model. With regard to scaling, the RFG model (by construction) scales with ψ (and of course with ζ or $y_{\rm RFG}$, since they are intrinsically related). It also scales quite well versus y. The HM scales very well with ψ' (by construction), but also quite well with ψ. In contrast, the QHD model does not scale with any of the above variables if the ratio m_N^*/m_N is constant and differs significantly from unity. One must conclude that the successful scaling behavior seen experimentally indicates that m_N^* must approach m_N as q increases beyond about 1 GeV/c.

Finally, we note that an exact CSR and exact scaling behavior should not be expected to occur. We certainly believe that interaction effects beyond those of the mean field (whose effects are incorporated at least to some extent in the models studied here) can play a role even at momentum transfers as high as 1 GeV/c. Furthermore, we expect that two-body meson exchange current effects can also play a role, for instance, making the longitudinal and transverse reduced responses scale to different functions. Both of these classes of corrections are currently being re-investigated.

ACKNOWLEDGMENTS

This work was supported in part by funds provided by the U.S. Department of Energy (D.O.E.) under cooperative research agreement #DF-FC02-94ER40818 and by the INFN-MIT "Bruno Rossi" Exchange Program.

REFERENCES

[1] R. Cenni, T.W. Donnelly and A. Molinari, Phys. Rev. **C56**, (1997) 276.

[2] P. Amore, R. Cenni, T.W. Donnelly and A. Molinari, Nucl. Phys. **A615**, (1997) 353.

[3] D.B. Day, J.S. McCarthy, T.W.Donnelly and I. Sick, Annu. Rev. Nucl. Part. Sci. **40**, (1990) 357.

[4] E. Pace and G. Salmè, Phys. Lett. **B110**, (1982) 411; C. Ciofi degli Atti, E. Pace and G. Salmè, Phys. Lett. **B127**, (1983) 303.

[5] W.M. Alberico, A Molinari, T.W. Donnelly, E.L. Kronenberg and J.W. Van Orden, Phys. Rev. **C38**, (1988) 1801.

[6] C.F. Williamson *et al.*, Phys. Rev. **C56**, (1997) 3152.

[7] T.W. Donnelly and I. Sick, (to be published).

[8] J. Jourdan, Phys. Lett. **B353**, (1995) 189; Nucl. Phys. **A603**, (1996) 117.

[9] B.D. Serot and J.D. Walecka, Advances in Nuclear Physics **16**, (1986) 1.

[10] H. Kim, C.J. Horowitz and M.R. Frank, Phys. Rev. **C51**, (1995) 792.

[11] T. De Forest, Jr., Nucl. Phys. **A392**, (1983) 232.

[12] J.A. McNeil *et al.*, Phys. Rev. **C34**, (1986) 746.

[13] M.B. Barbaro, A. De Pace, T.W. Donnelly and A. Molinari, Nucl. Phys. **A569**, (1994) 701.

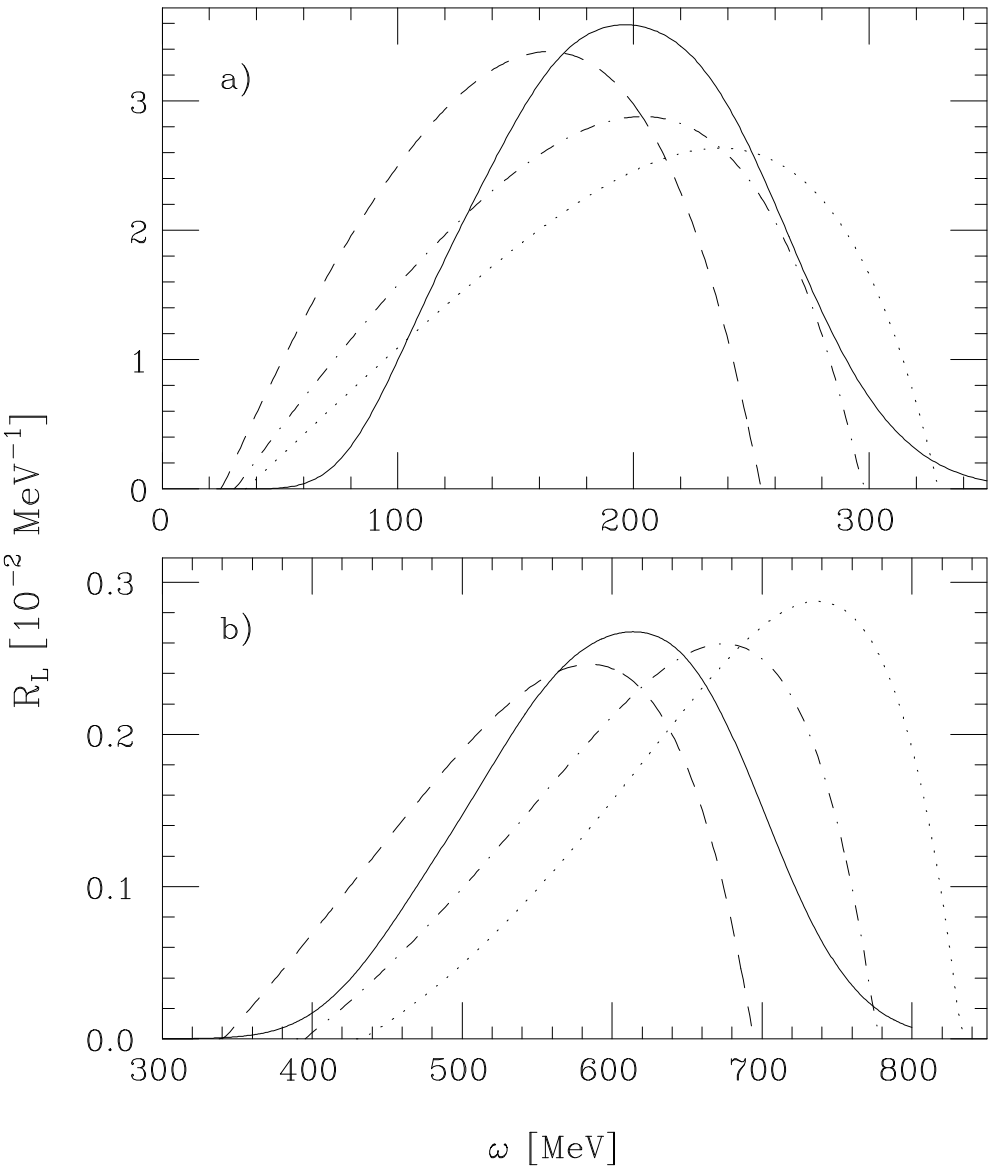

FIG. 1. The longitudinal response function R_L is displayed versus ω for q = 0.55 GeV/c in panel (a) and q = 1.14 GeV/c in panel (b). The four curves shown are the following: dashed — RFG, solid — HM, dot-dashed — QHD model (m_N^*=0.8 m_N) and dotted — (m_N^*=0.68 m_N). Here and in all of the following figures the nucleus chosen is ^{40}Ca. For the RFG and QHD models we always assume k_F=230 MeV/c, while the HM parameters are discussed in the text.

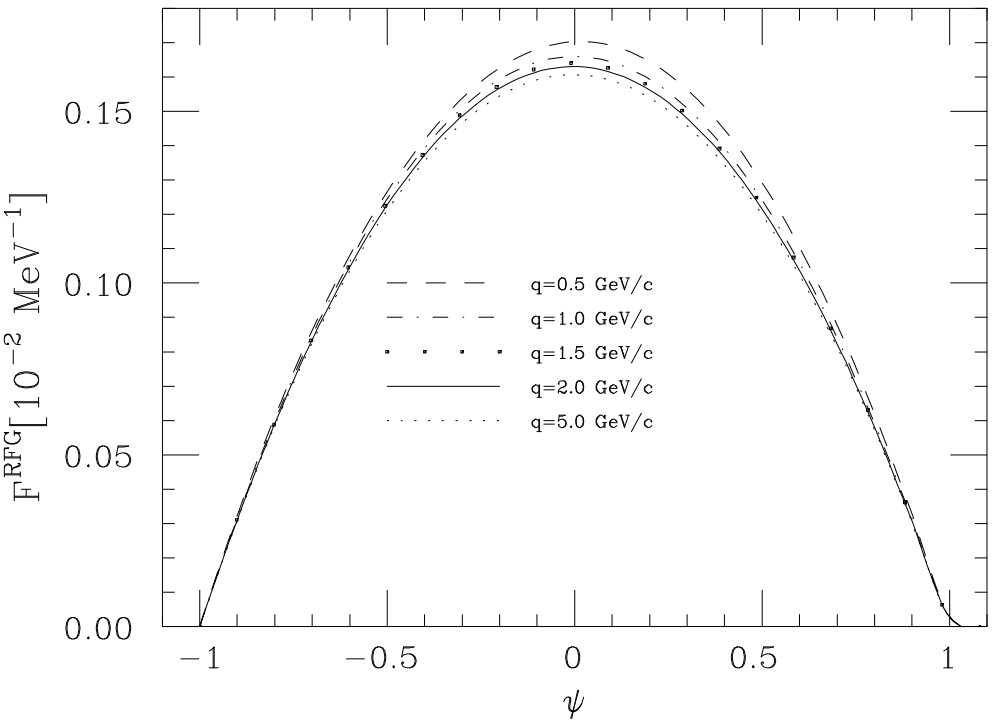

FIG. 2. Scaling is shown as a function of ψ using the RFG cross section at 10^o scattering angle divided by the off-shell cc1 form with separation energy $E_S = 8$ MeV for a wide range of momentum transfers.

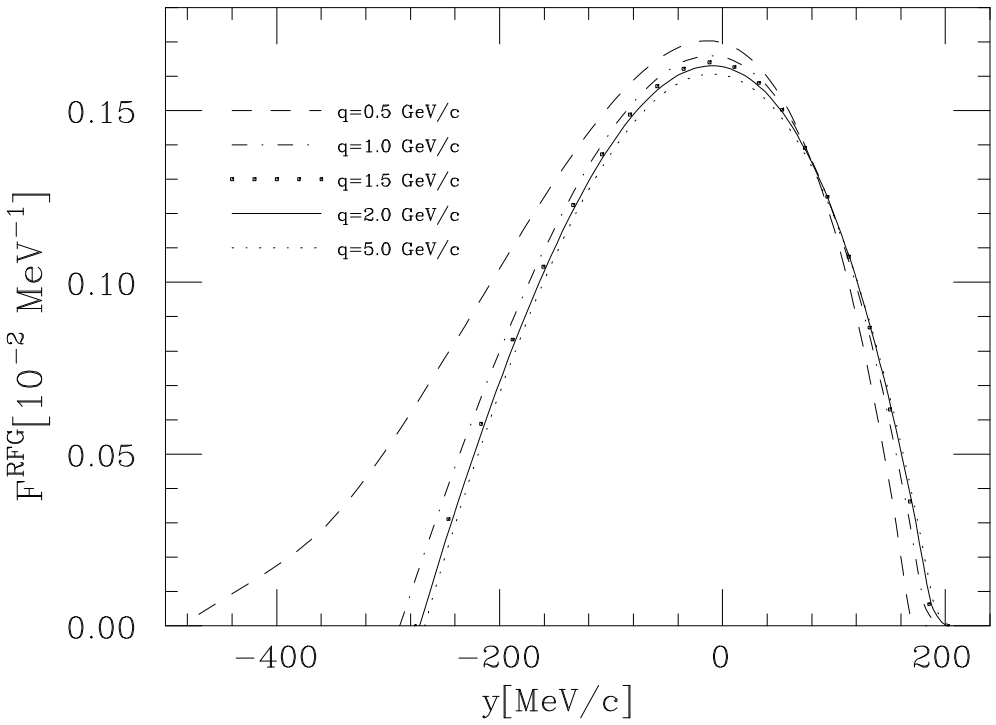

FIG. 3. The scaling function F^{RFG} is shown for the same conditions employed in Fig. 2 as a function of the y-scaling variable defined in Eq. (2.2), rather than as a function of ψ (see Eq. (2.18)) in which it scales exactly, by construction. The separation energy occurring in the definition of y has been set to 8 MeV for these results.

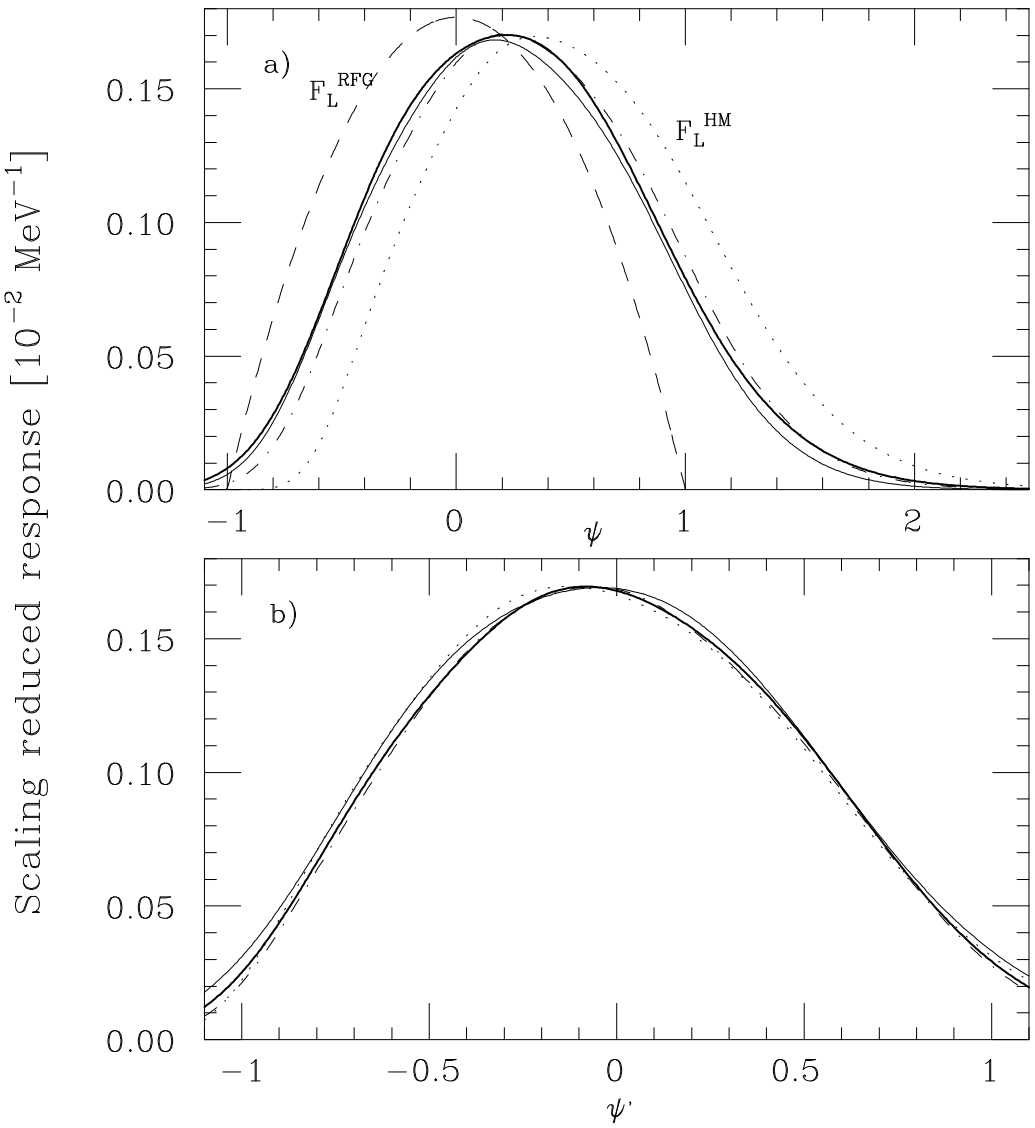

FIG. 4. The reduced response $F_L^{\rm HM}$ (the hybrid model scaling function) is shown as a function of ψ in panel (a) and ψ' in panel (b) for 4 values of q (fine dotted — 0.5, dot-dashed — 1.0, heavy solid — 1.5 and solid — 2.0 GeV/c). The RFG result, which scales exactly as a function of ψ, is also shown for reference as a dashed curve in panel (a).

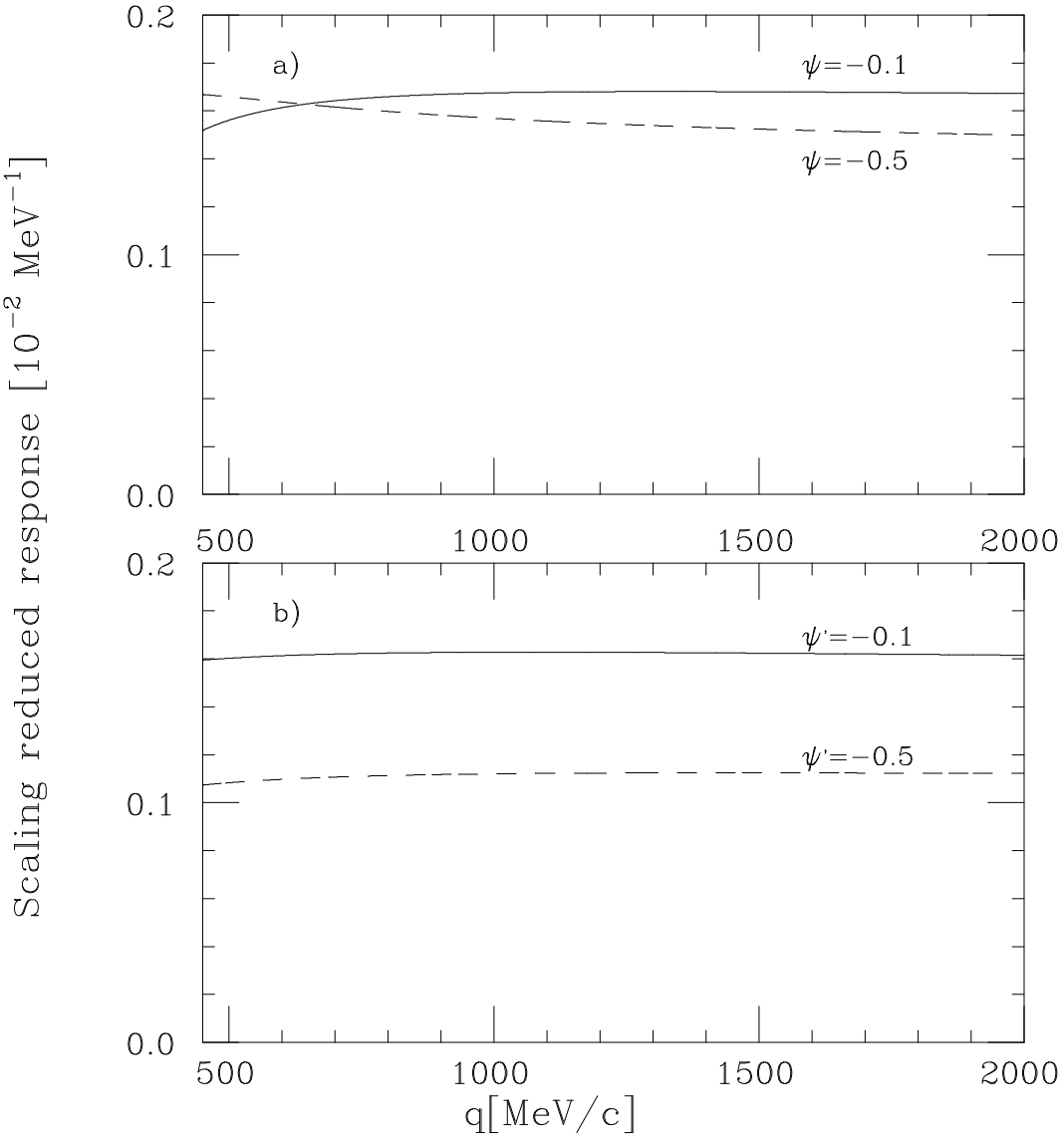

FIG. 5. The reduced response $F_L^{\rm HM}$ is shown as a function of q at $\psi = -0.1$ and -0.5 in panel (a) and at $\psi' = -0.1$ and -0.5 in panel (b).

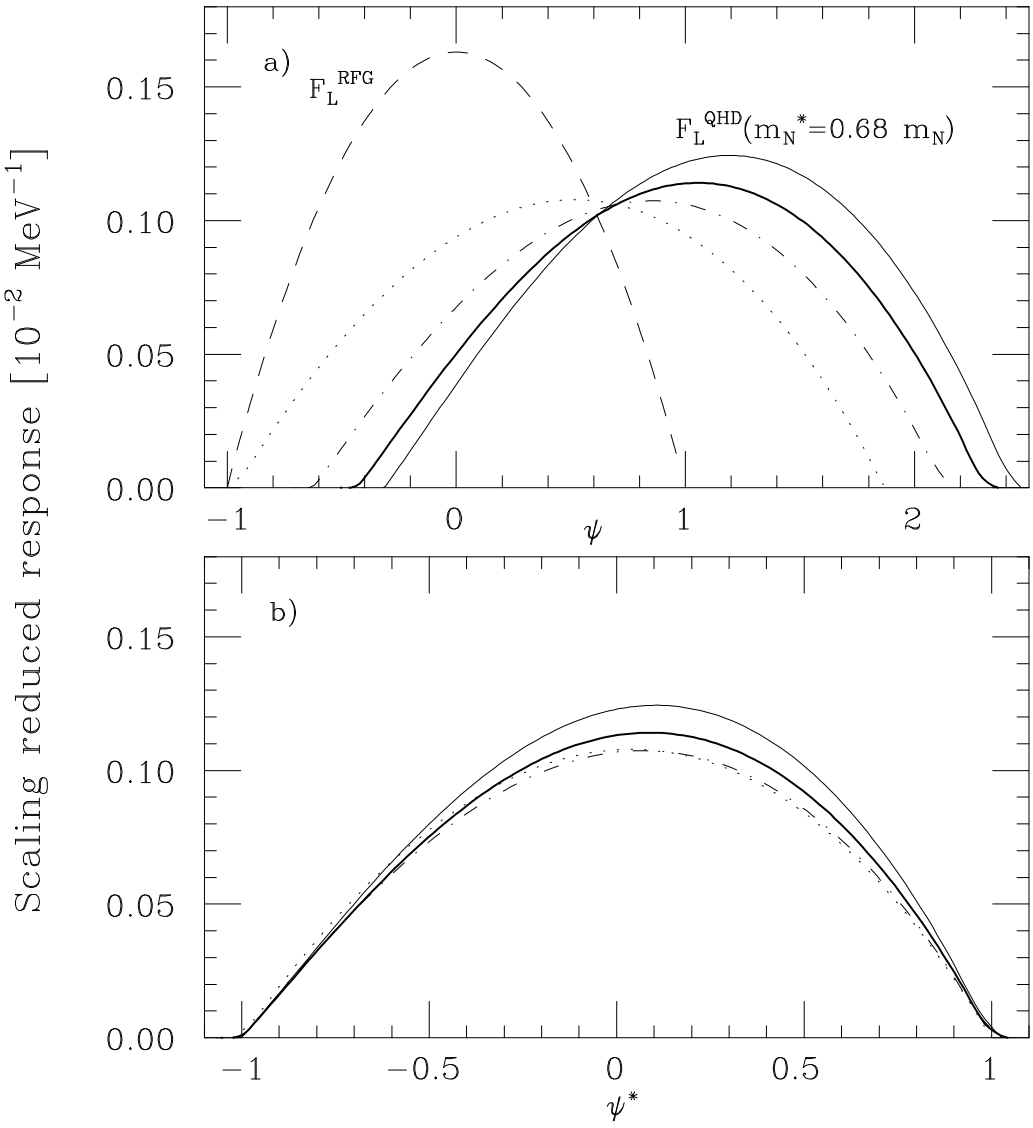

FIG. 6. The reduced response $F_L^{\rm QHD}$ with $m_N^* = 0.68\ m_N$ is shown as a function of ψ in panel (a) and ψ^* in panel (b) for 4 values of q (fine dotted — 0.5, dot-dashed — 1.0, heavy solid — 1.5 and solid — 2.0 GeV/c). The RFG result, which scales exactly as a function of ψ, is also shown for reference as a dashed curve in panel (a).

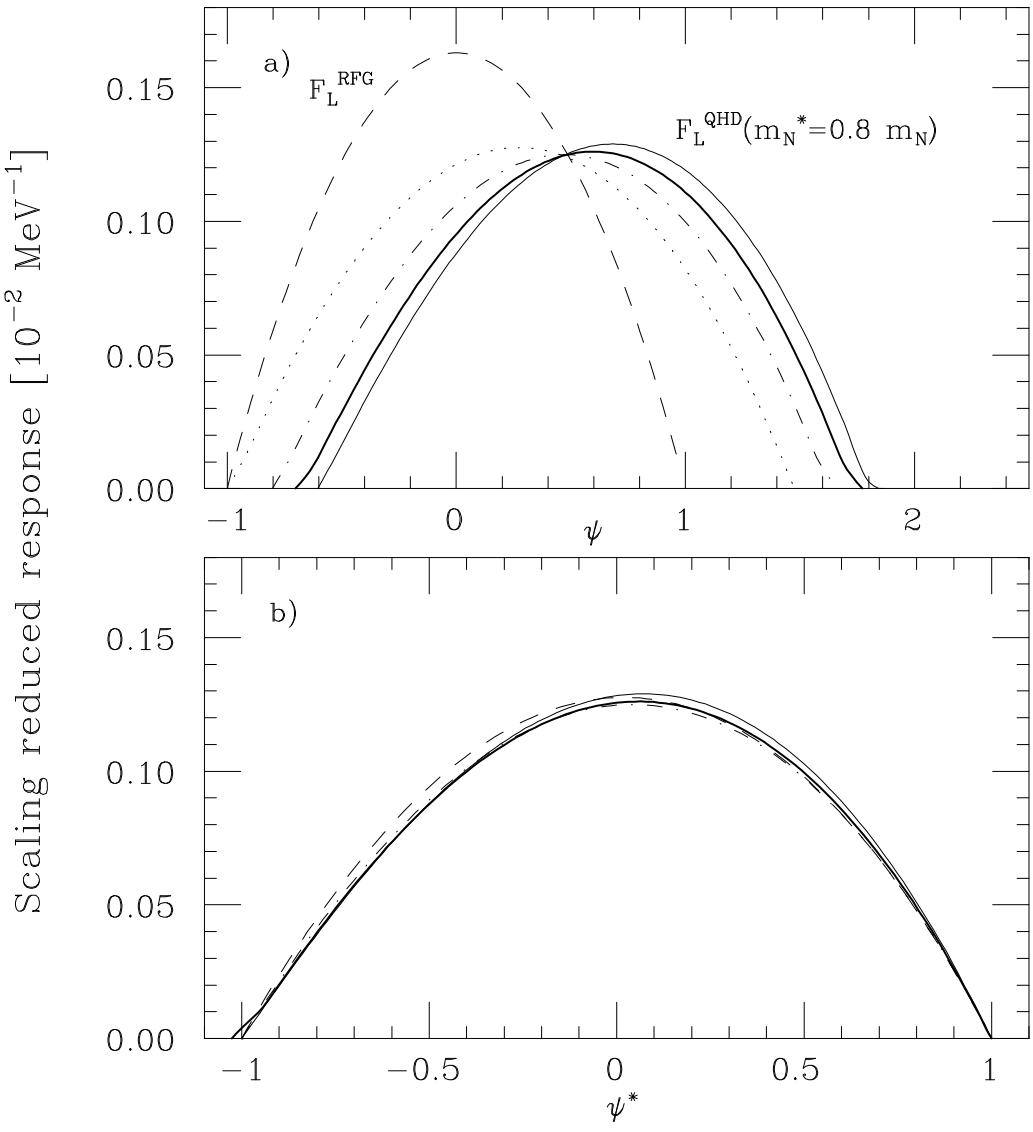

FIG. 7. As in Fig. 6, except now with $m_N^* = 0.68\, m_N$

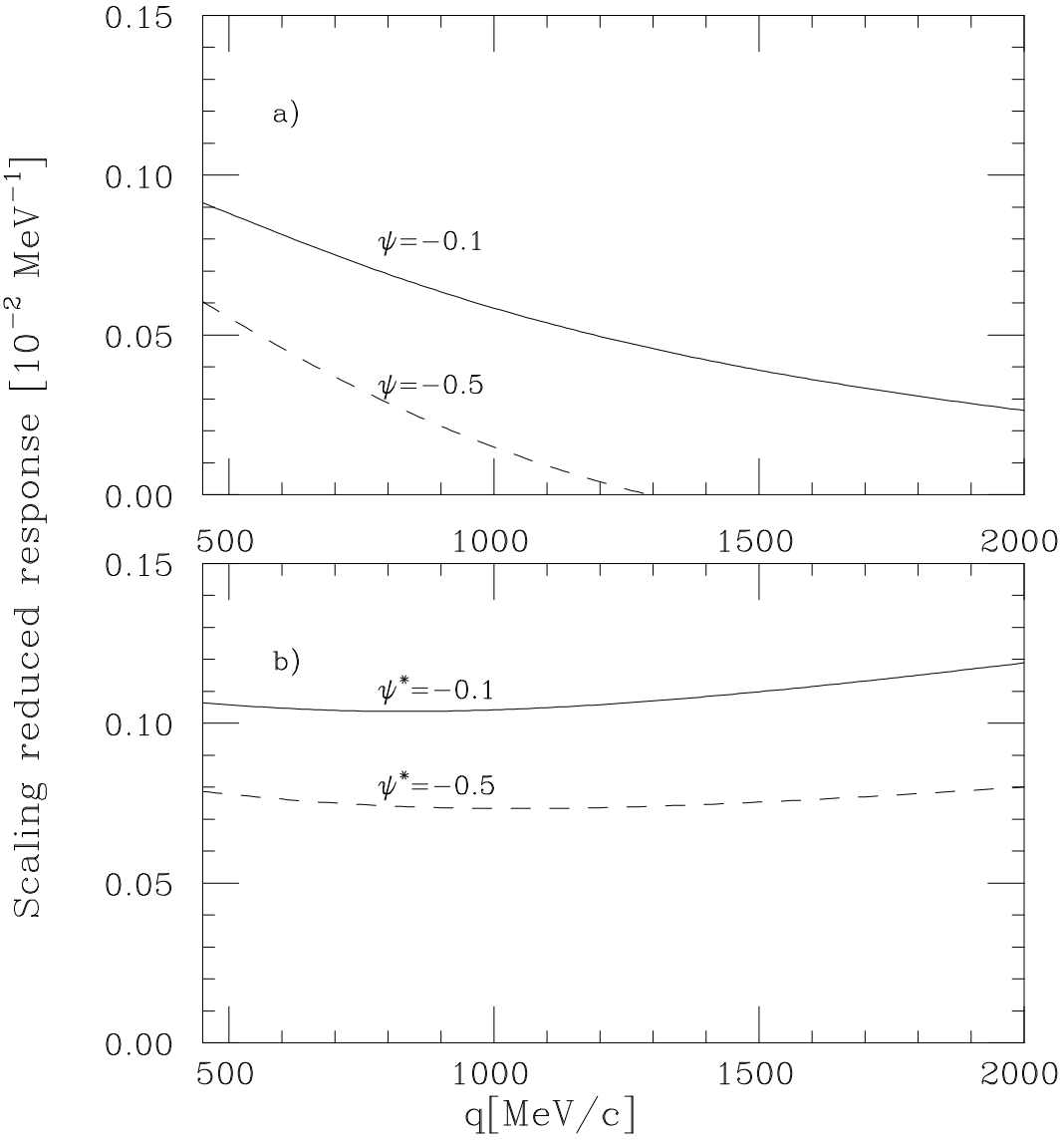

FIG. 8. The reduced response $F_L^{\rm QHD}$ is shown as a function of q at $\psi = -0.1$ and -0.5 in panel (a) and at $\psi^* = -0.1$ and -0.5 in panel (b).

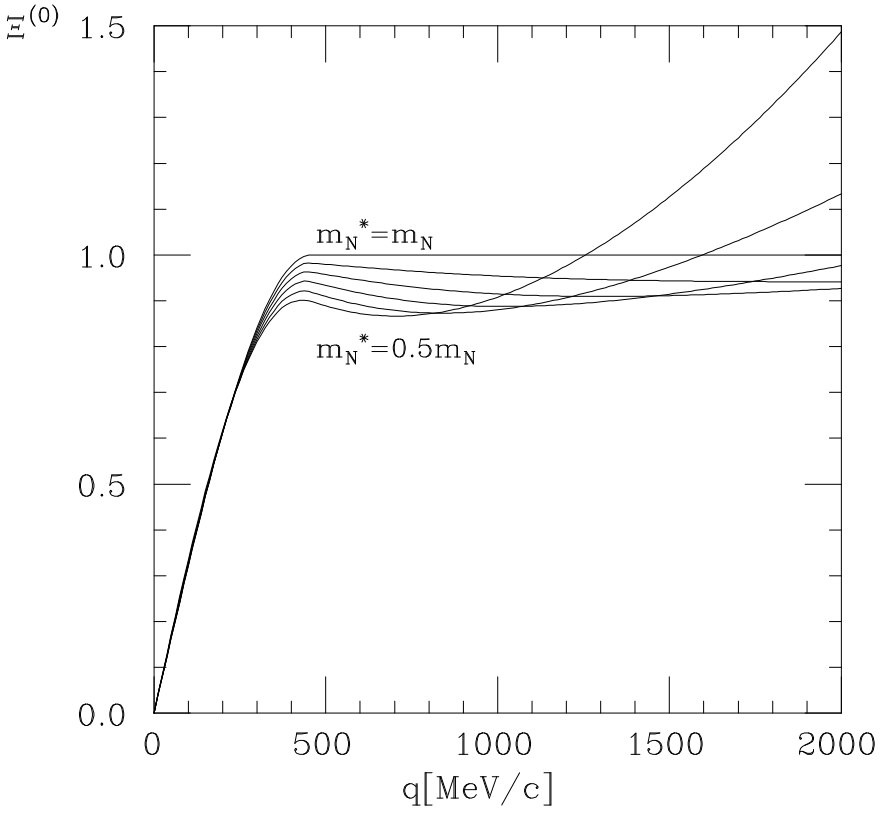

FIG. 9. Coulomb sum rule $\Xi^{(0),\mathrm{QHD}}$ of the QHD model is shown as a function of q for different values of the effective mass m_N^*, ranging from 1 to 0.5 m_N in steps of 0.1 m_N.

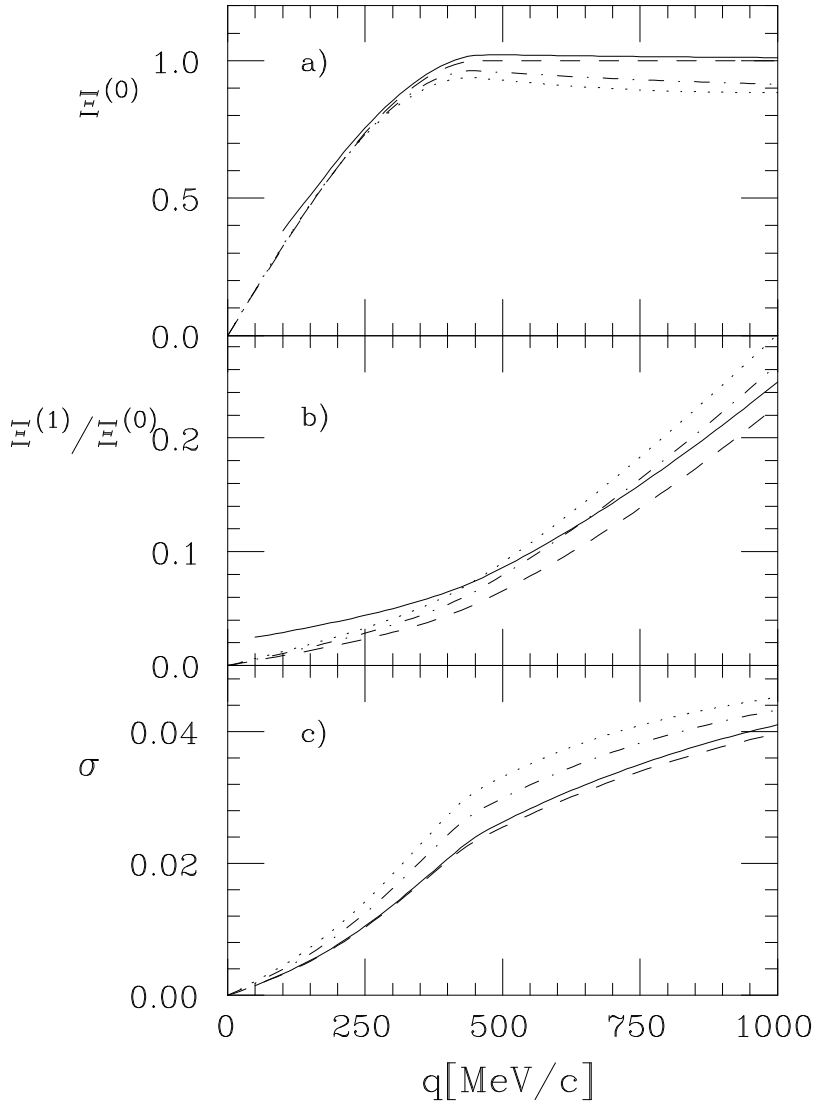

FIG. 10. The Coulomb sum rule (a), energy-weighted sum rule (b) and variance (c) are shown as functions of q for the three models employed in this work: dashed — the RFG, solid — the HM and the QHD model with m_N^*=0.8 m_N (dot-dashed) and 0.68 m_N (dotted).

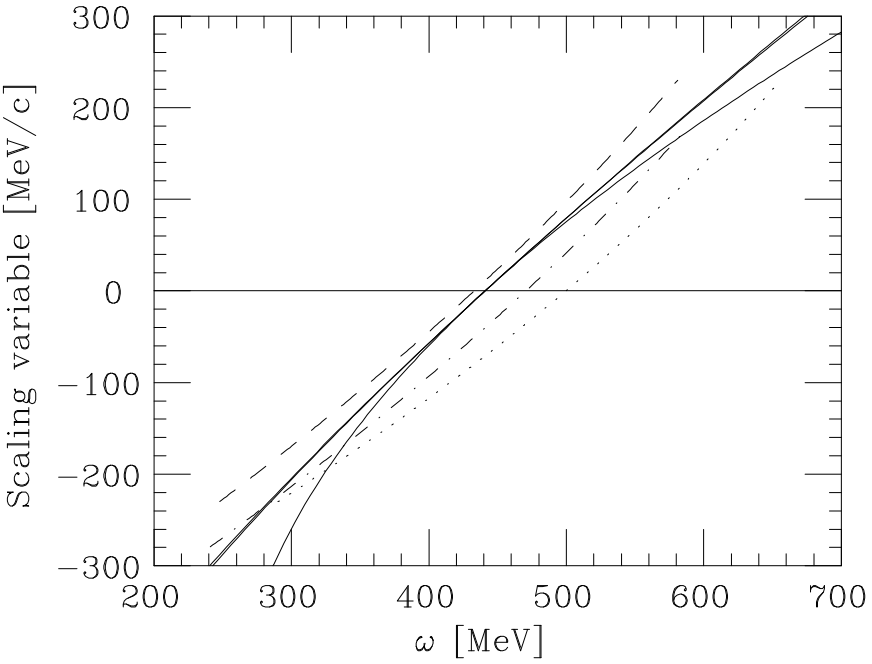

FIG. 11. The various scaling variables employed in this work are shown as functions of ω at $q = 1$ GeV/c: $k_F\psi$ (dashed), $k_F(HM)\psi'$ with $k_F(HM) = 237$ MeV/c (dot-dashed), $k_F\psi^*$ (dotted) and y (solid). The three solid curves correspond to $A = 2$, 20 and 200, respectively, starting from below.